Fish-on-Chips: An optofluidic platform to investigate the neural and chemosensory axes of zebrafish

January 27 2023, by Thamarasee Jeewandara

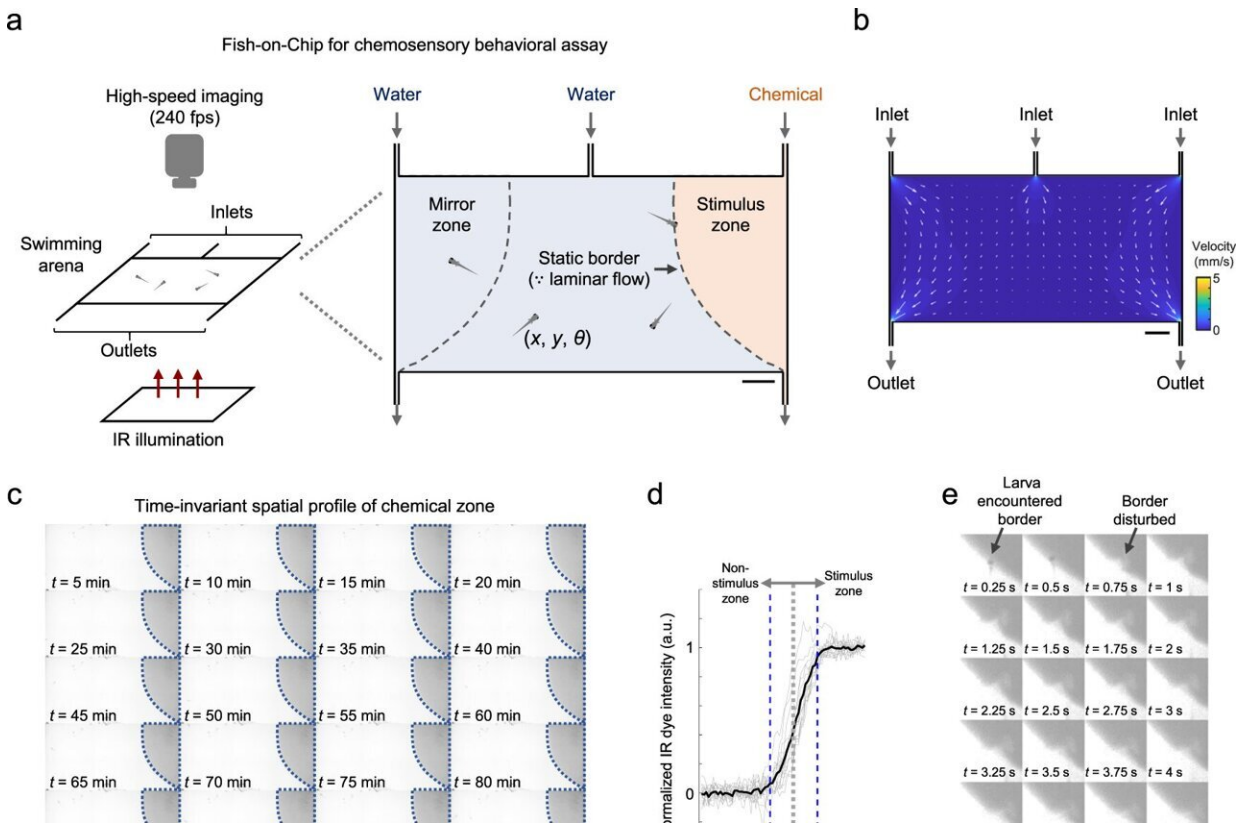

A fluidics-based swimming arena for chemosensory behavioral assay. a) Schematics of the chemosensory behavioral assay. Zebrafish larvae swimming in a two-dimensional arena (60 mm × 30 mm × 1.5 mm) are imaged at high speed (240 fps) under infrared (IR) illumination in the absence of visible light. A chemical zone (stimulus zone) is created and maintained by a constant slow inflow of a given chemical (dissolved in water) via the rightmost fluid inlet.

Assays in which all zones are filled by water streams serve as control. The symmetrical mirror zone serves as an additional control for obtaining baseline behaviors when infused by water. The laminar flow maintains a static border between the zones. The coordinates (x, y) and orientation (θ) of the center of the head are tracked and analyzed for each larval zebrafish. b) Simulated fluid velocity profile in the swimming arena. Vectors show the direction of flow at the respective locations, with length scaling according to the relative magnitude of velocity. The absolute magnitude of velocity is color-coded according to the color scale bar. c) Time-lapsed images (contrast-enhanced) showing the chemical zone border in the presence of larval zebrafish with an IR dye flowing in via the rightmost fluid inlet in a swimming arena identical to that used for chemosensory behavioral assays. Dotted lines in each image outline the same border. Note the subtle differences between the images showing zebrafish larvae navigating the arena. d) Individual line profiles (gray) of IR dye intensity along normal vectors at different spatial locations of the chemical border and their mean (black). Positive and negative values on the x axis indicate distances from the border further into and away from the stimulus side, respectively. Blue dashed lines mark ± 1 mm from the border. e Time-lapsed images (contrast-enhanced) showing transient border disturbance and restoration in an example larval zebrafish border-crossing event. Scale bars in a–c and e: 0.5 cm. Source data are provided as a Source Data file. Credit: *Nature Communications* (2023). DOI: 10.1038/s41467-023-35836-2

Neuroscientists study chemosensory processing by establishing chemical cues and the corresponding behavioral responses to record large-scale neuronal activity. In a new report now published in *Nature Communications*, Samuel Sy and a team of scientists in neurology, health sciences, biomedical engineering and mathematics in China and France presented a new method based on a set of optofluidic tools. This technology established chemical delivery to simultaneously image the behavioral outputs and whole-brain neural activities at cellular resolution in larval zebrafish.

The team included a fluidics-based swimming arena within the experimental setup and an integrated microfluidics-light sheet fluorescence microscopy system. The technical methods incorporated laminar fluid flow to achieve chemical cue representation. The team named the new technique "Fish-on-Chips," which is now ready to empower investigations of neural coding in the chemical senses.

Systems-level investigations of the brain

Neuroscientists explore the brain to understand behavioral goals of animals and comprehend the underlying algorithmic and neuronal mechanisms. Researchers have thus far developed a variety of sophisticated tools to mimic the natural habitats and thereby reconstruct the sensory environments of an animal for behavioral analysis at cellular resolution. For example, larval zebrafish are attractive vertebrates due to their capacity to rapidly acquire innate chemosensory, auditory and visually guided behaviors.

Evolutionarily, chemosensation is the oldest existing sensory system, and researchers have made considerable efforts to understand the behaviors underlying neural basis in a variety of popular model organisms in systems neuroscience.

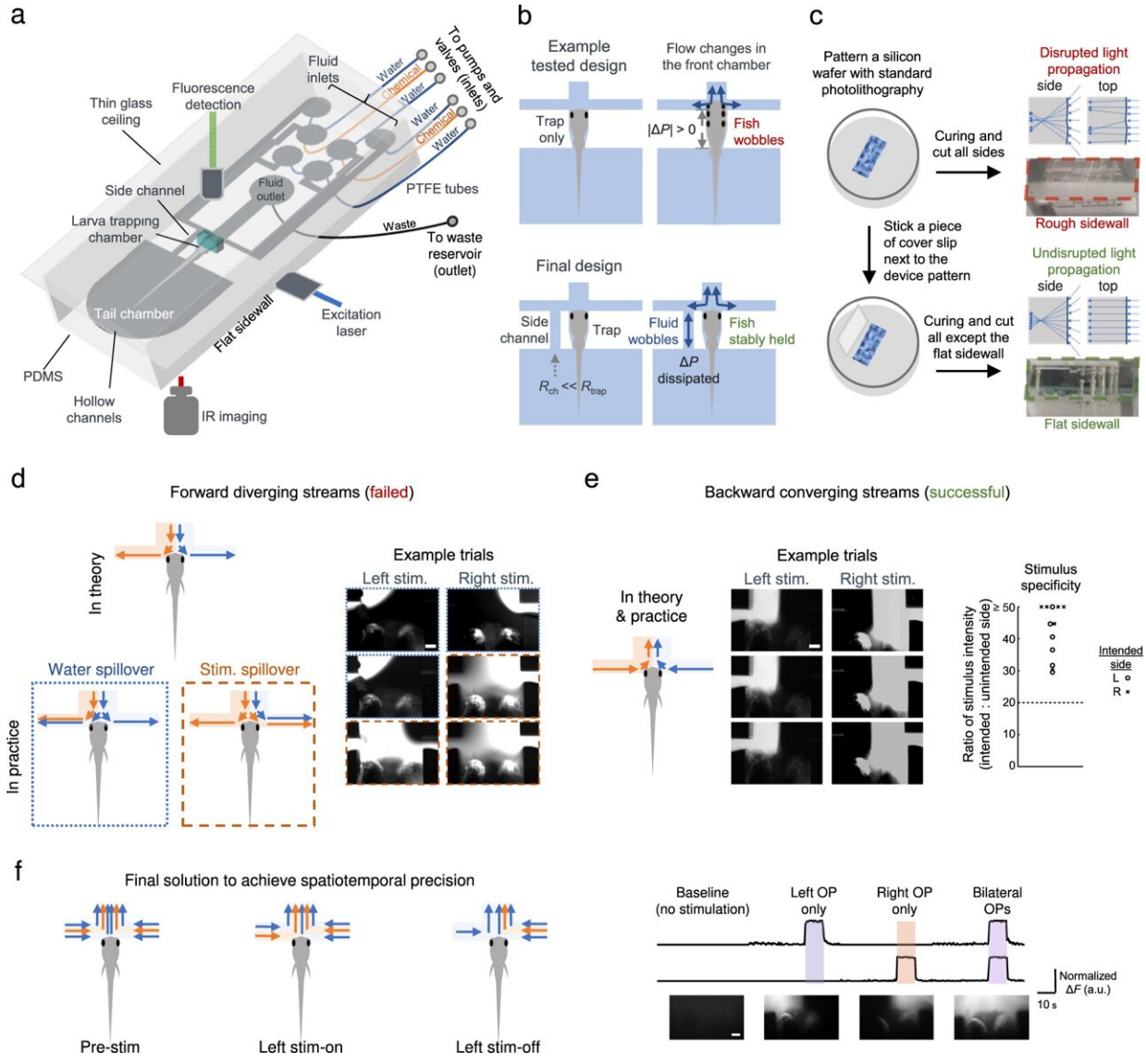

Design principles of the microfluidic components of the optofluidic system. a) Schematics of the PDMS microfluidic (μfluidic) module with a larval chamber, a tail chamber, and a fluid delivery front chamber, which was made compatible with whole-brain and tail imaging. b) Upper panel: when there are flow changes in the front chamber, changes in pressure difference across the front and tail chambers (ΔP) leads to larva wobbling. Lower panel: with the addition of a side channel that has a much smaller fluid resistance (Rch) than that of the trapping chamber (Rtrap), fluid in the side channel dissipates the changes in ΔP and the larva is stably held. Also see Supplementary Fig. 2e, f. c) In contrast to rough sidewalls, the flat sidewall ensures undisrupted excitation laser propagation and light sheet formation. The sidewalls are outlined by dashed lines. Schematic side

and top views of light ray propagations are shown. d) Left panel: schematic depictions of the theoretical and actual fluid segregation using forward diverging streams (left-side stimulation illustrated). Blue: water. Orange: chemical (Stim.). Arrows indicate the flow directions. Right panel: example images showing contralateral spillover of chemical or water (specified using corresponding image outlines). e) Left panel: schematic depictions of the fluid segregation using backward converging streams (left-side stimulation illustrated). Middle panel: example images. Right panel: the ratio of stimulus intensity (intended side vs. unintended side) in test trials (n = 12 trials in 2 larvae), quantified with fluorescent imaging using 100 μM fluorescein in the chemical stream. All recorded ratios were >20 (dashed line). Images in d and e were acquired with three trials for each side with a larva. Scale bars in d and e: 100 μm. f) Left panel: the fluidic streams layout that was implemented during different periods of unilateral stimulus delivery (left-side stimulation illustrated). Right panel: visualization and monitoring of nasal stimulation by fluorescence imaging of 1 μM fluorescein in the vicinity of each OPs. Images show one trial for each case with a larva. Scale bar: 100 μm. Source data are provided as a Source Data file. Credit: *Nature Communications* (2023). DOI: https://doi.org/10.1038/s41467-023-35836-2

While fluidics and microfluidics provide precise fluid regulation to study chemosensation, a custom microfluidics-integrated light-sheet fluorescence microscope can establish whole-brain neuronal activity imaging at cellular resolution. In this report, Sy and colleagues therefore used a fluidics and microfluidics-based method alongside a microfluidics-integrated light sheet fluorescence microscope to study chemosensation for chemical cue delivery in small animals.

Chemosensory behavioral assays

To understand chemosensory-guided behavior under biomimicry, the team established a behavioral assay for larval zebrafish with a precisely defined arena in which the concentration profile of a chemical remained

constant. The team maintained equal flow rates for all three inlets to establish clear separation of fluidic stream zones in the presence of actively swimming larvae.

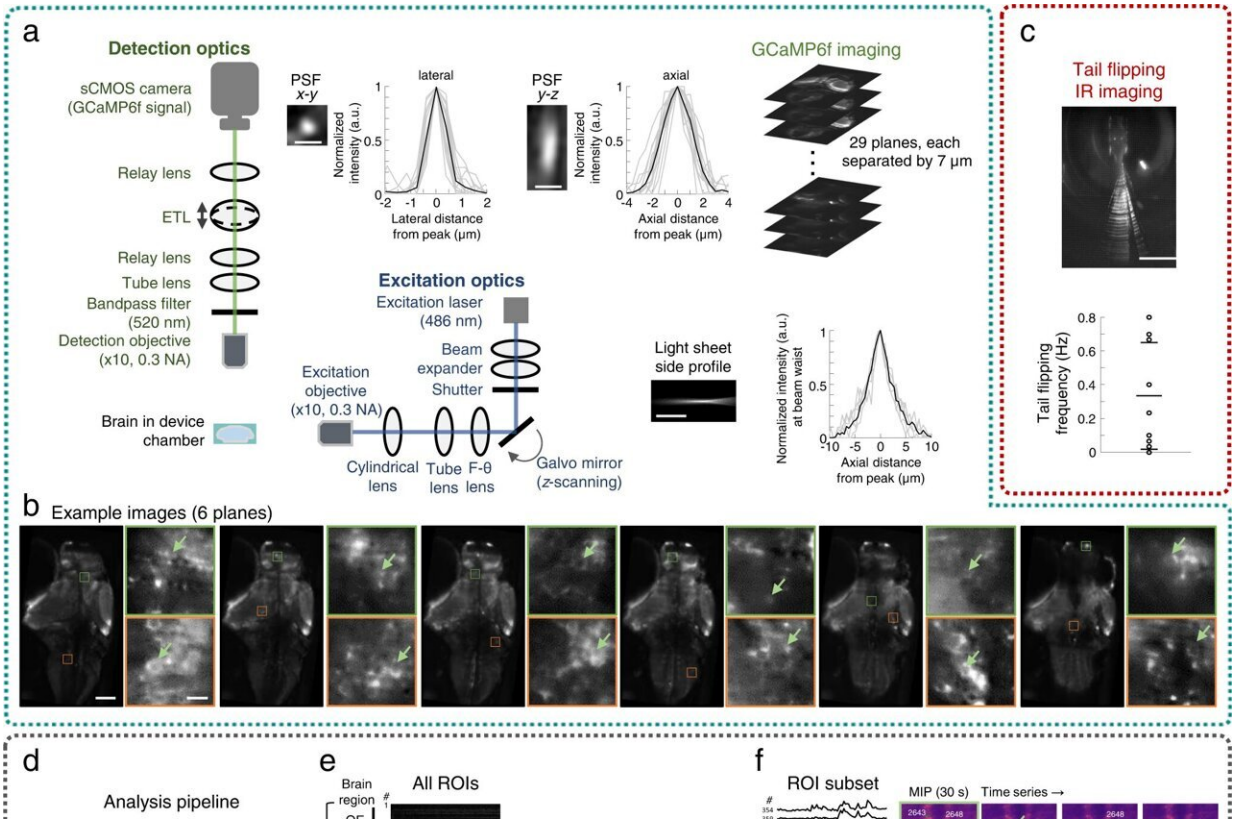

An integrated optofluidic system for in vivo imaging of chemosensory-evoked neuronal activity and behavior. a) The microfluidic (μfluidic) module is integrated with a scanning light sheet microscope for whole-brain imaging in larval zebrafish. Inset image/plot sets show characterization of the excitation and detection arms (see "Methods"). Each set includes an image showing one example profile and a plot of profiles (gray: individual; black: mean), for the lateral (x–y) and axial (y–z) point spread functions (PSFs, scale bars: 2 μm), and the light sheet side profile (scale bar: 50 μm). b) Example image planes. For each set, the two images on the right are enlarged and contrast-adjusted from the outlined areas of the corresponding larger images. Scale bars: 100 μm for the larger images and 10 μm for the zoomed-in images. Arrows indicate example neurons at various brain locations. c) Upper panel: temporally overlaid tail

images of an example larva (scale bar: 1 mm). Lower panel: spontaneous tail flipping frequency of 9 larvae that were behaviorally active. Horizontal lines indicate mean ±1 SD. d) Workflow of the custom-developed data analysis pipeline. e) Brainwide spontaneous activity heatmap and region-of-interest (ROI) maps (projected to coronal, transverse, and sagittal planes) from an example larva, with 3768 extracted ROIs (each corresponding to a neuron and color-coded by ROI number. Simultaneously acquired tail flipping recording and an example tail flipping event are shown below. Horizontal scale bars for the heatmap: 5 seconds. Scale bars for the event plot: 50 milliseconds (horizontal) and 10° (vertical). Scale bars for the brain maps: 50 μm in Z-Brain atlas space. f) Left panel: The calcium signal traces of 48 example neurons. Scale bar: 5 seconds. Right panel: a maximum intensity projection (MIP) and the time-series images of the first 30-second interval at a hindbrain region with 6 highlighted ROIs (green: ROI masks). Arrows indicate the locations and times of each ROIs near a calcium event's peak. Brain region abbreviations: OE olfactory epithelium, OB olfactory bulb, Pa pallium, sPa subpallium, Hb habenula, PO preoptic area, Di diencephalon, Me mesencephalon, Ce cerebellum, Rh rhombencephalon. Scale bar for the MIP and time-series images: 50 μm. Source data are provided as a Source Data file. Credit: *Nature Communications* (2023). DOI: 10.1038/s41467-023-35836-2

Additionally, the researchers uncovered the circuit principles of chemosensory processing to deliver chemical stimuli while simultaneously recording neuronal activity. They accomplished this by stabilizing the larval subjects to establish compatibility with neuronal imaging methods while precisely regulating the delivery of a chemical stimuli. They also designed a light sheet fluorescence microscope-compatible microfluidic chip to stabilize the larvae for high-quality neuronal activity imaging and thereby ensured microfluidic chip compatibility.

Imaging neuronal activities and behavior

The research team next sought to stably integrate the microfluidic components with a custom-built light sheet fluorescence microscope for additional experiments. Using the platform, they examined nine behaviorally active larvae with spontaneous tail flipping frequency for behavioral recording and chemosensory activities, as well as associated neuronal behavior at cellular resolution within the Fish-on-Chips navigation arena. The scientists also explored chemosensory behavioral algorithms underlying the species during cadaveric avoidance, where the model organisms relied on binasal inputs.

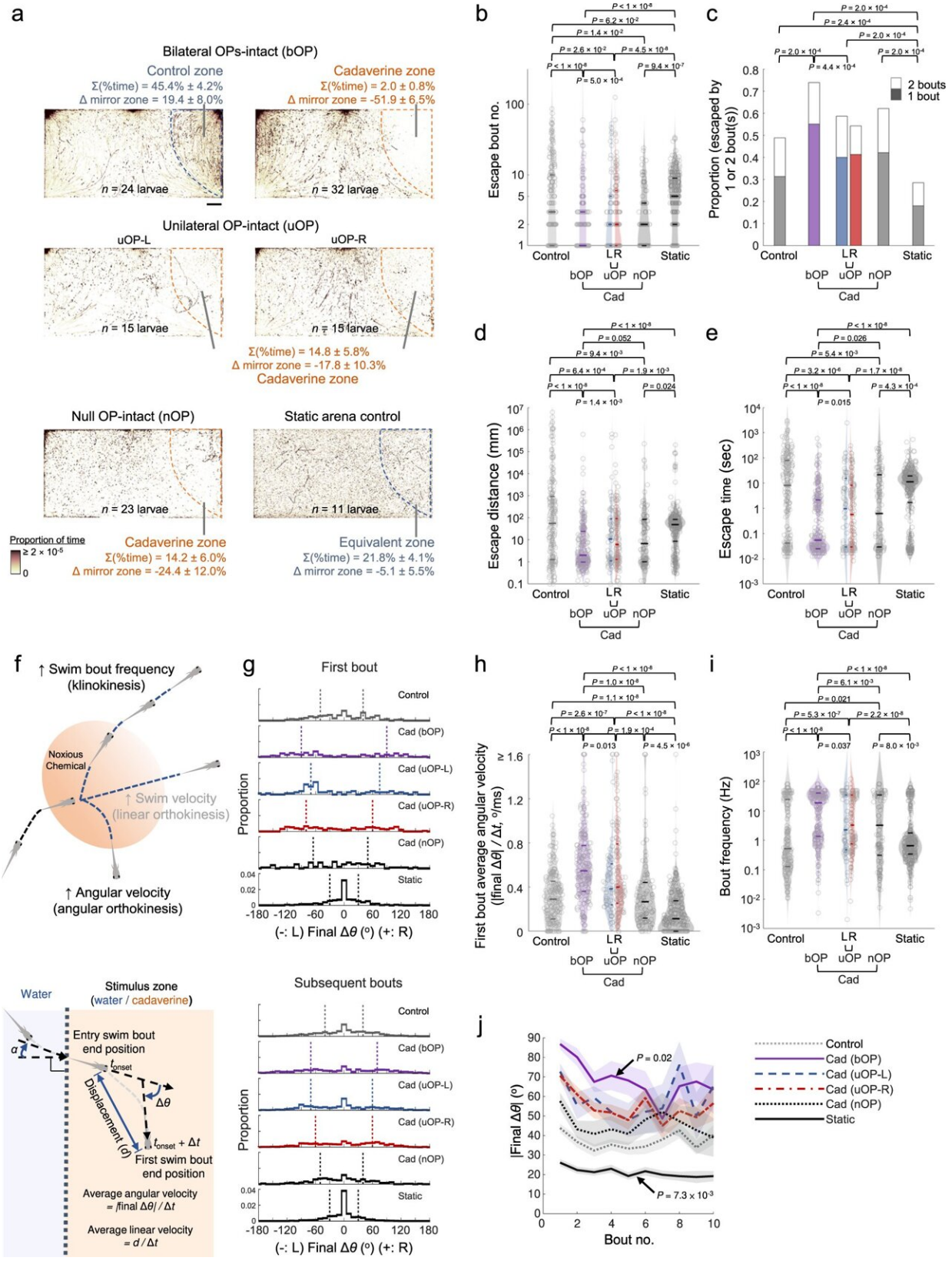
a
Bilateral OPs-intact (bOP)
Control zone
Σ(%time) = 45.4% ± 4.2%
Δ mirror zone = 19.4 ± 8.0%
Cadaverine zone
Σ(%time) = 2.0 ± 0.8%
Δ mirror zone = -51.9 ± 6.5%
n = 24 larvae
n = 32 larvae
Unilateral OP-intact (uOP)
uOP-L
uOP-R
n = 15 larvae
n = 15 larvae
Σ(%time) = 14.8 ± 5.8%
Δ mirror zone = -17.8 ± 10.3%
Cadaverine zone
Null OP-intact (nOP)
Static arena control
n = 23 larvae
n = 11 larvae
Proportion of time
≥ 2 × 10-5
0
Cadaverine zone
Σ(%time) = 14.2 ± 6.0%
Δ mirror zone = -24.4 ± 12.0%
Equivalent zone
Σ(%time) = 21.8% ± 4.1%
Δ mirror zone = -5.1 ± 5.5%
b
Escape bout no.
Control
LR
Static
bOP uOP nOP
Cad
c
Proportion (escaped by 1 or 2 bout(s))
2 bouts
1 bout
d
Escape distance (mm)
e
Escape time (sec)
f
↑ Swim bout frequency (klinokinesis)
Noxious Chemical
↑ Swim velocity (linear orthokinesis)
↑ Angular velocity (angular orthokinesis)
Water
Stimulus zone (water / cadaverine)
Entry swim bout end position
Displacement (d)
Δθ
First swim bout end position
Average angular velocity = |final Δθ| / Δt
Average linear velocity = d / Δt
g
First bout
Subsequent bouts
Control
Cad (bOP)
Cad (uOP-L)
Cad (uOP-R)
Cad (nOP)
Static
Proportion
(-: L) Final Δθ (°) (+: R)
h
First bout average angular velocity (|final Δθ| / Δt, °/ms)
i
Bout frequency (Hz)
j
|Final Δθ| (°)
Bout no.
Control
Cad (bOP)
Cad (uOP-L)
Cad (uOP-R)
Cad (nOP)
Static

Larval zebrafish cadaverine avoidance revealed by the chemosensory behavioral assay. a) Upper panels: footprints of bilateral OP-intact (bOP) larvae in control and avoidance assays. Middle panels: footprints of unilateral OP-intact (uOP) larvae in avoidance assays. Lower panels: footprints of null OP-intact (nOP) larvae in avoidance assays and static arena control groups. Note that the static arena control group assays were carried out without flow. For each group, the rightmost (stimulus or water) zones are outlined by dashed lines. The percentages of time spent in the rightmost zone and their differences from that in the mirror water zone (Δ mirror zone) are shown (with SEMs across assays). Scale bar: 0.5 cm. b) Bout number, c proportion of entry-to-exit events with only 1 or 2 bouts (P value: one-sided Chi-squared test with Tukey's post-hoc test, comparing 2-bout event proportions), d distance traveled, and e time taken to escape the rightmost zone in control assays (Control: bOP larvae in the water-only arena with flow; Static: bOP larvae in water-only arena without flow) and avoidance assays (bOP larvae, left OP-intact (L) or right OP-intact (R) uOP larvae, and nOP larvae in arenas with cadaverine stream in the stimulus zone). f Upper panel: illustration of navigational strategies that may be adopted after encountering a noxious chemical. Lower panel: schematics of kinematic parameters that can be extracted. | | denotes absolute value. g Histograms of turn angle distributions of first (upper) and subsequent (lower) bouts (i.e., final Δθ). h First bout average angular velocity (i.e., |final Δθ|/Δt) upon entering the rightmost zone. i Swim bout frequency quantified from all rightmost zone entry-to-escape trajectories. j |Final Δθ| vs. bout number (line: mean; shadow: SEM) after rightmost zone entry. P value: two-sided Mann–Kendall trend test. b, d, e, i The parameters are plotted in log scales. In b, d, e, h and i Horizontal lines indicate the medians, 75 and 25 percentiles for each group. Shadows of the violin plots scale according to the probability density function. P values: Kruskal–Wallis test with Tukey's post hoc test. In a–e and g–j, numbers of assays, larvae, and rightmost zone border-crossing events: bOP (control): 6, 24, 211; bOP (avoidance): 8, 32, 251; uOP-L: 4, 15, 71; uOP-R: 4, 15, 155; nOP: 7, 23, 96; bOP Static: 3, 11, 283. Source data are provided as a Source Data file. Credit: *Nature Communications* (2023). DOI: 10.1038/s41467-023-35836-2

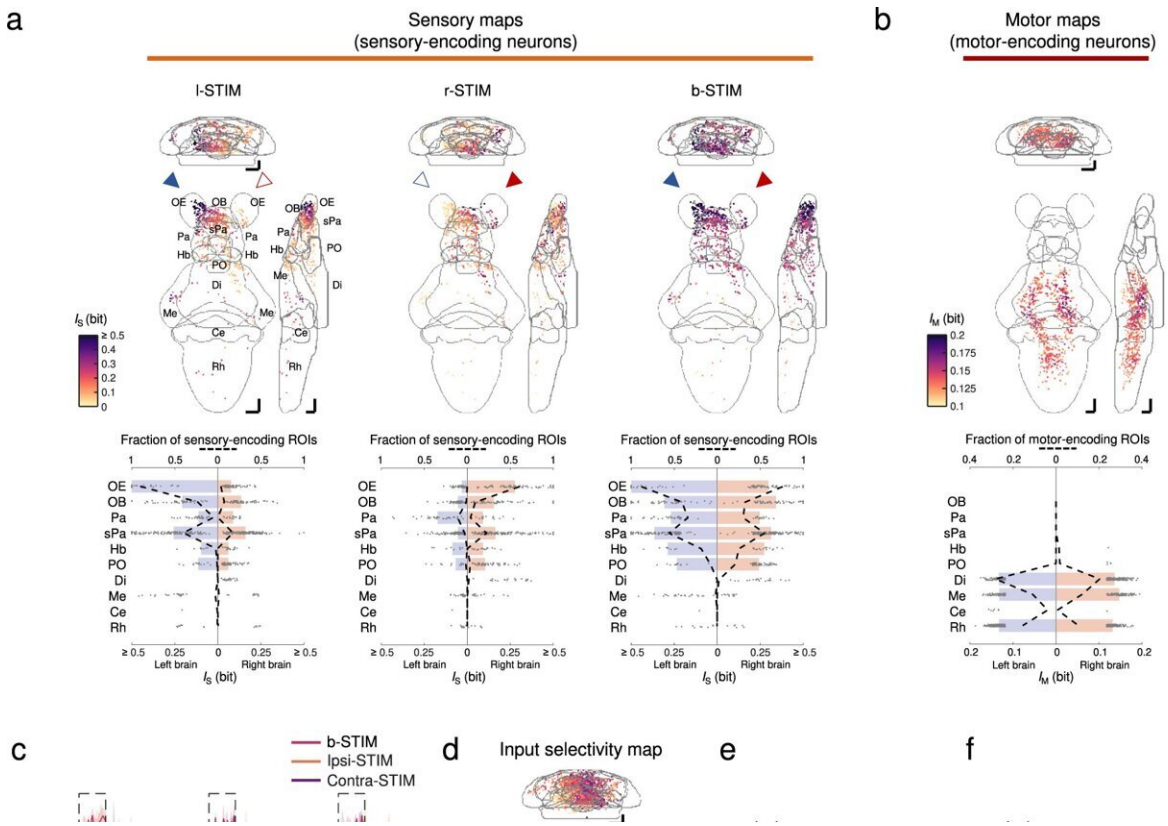

Brainwide neuronal activities evoked by chemosensory signals. a Upper panels: mean intensity projections (to coronal, transverse, and sagittal planes) of the mutual information between the calcium signals of regions-of-interest (ROIs) and stimulus profile of l-STIM (left panel), r-STIM (middle panel) or b-STIM (right panel) (IS), from an example larva. Solid triangles mark the corresponding OP(s) stimulated. Lower panels: corresponding brainwide IS distributions. Dashed lines indicate sensory-encoding ROI fractions. Bars represent the medians in regions with top six fractions of sensory-encoding ROIs with b-STIM. Abbreviations of brain regions: same as in Fig. 3e. b Upper panel: mean intensity projections of mutual information between the calcium signals of ROIs and tail flipping frequency (IM) from the larva in a. Lower panel: corresponding brainwide IM distribution. Dashed lines indicate motor-encoding ROIs fractions. Bars represent the medians in regions with top three fractions of motor-encoding ROIs. a, b The numbers of sensory-encoding and motor-encoding ROIs are 676 and 763, respectively. c Example trial-averaged responses to ipsilateral (ipsi-STIM, orange), contralateral (contra-STIM, violet), or bilateral (b-STIM, cherry) olfactory stimulation (n = 3 trials for each case) of individual ROIs from the

designated brain regions with a range of ipsilateral-contralateral input selectivity (first number) and fraction of nonlinear information (FIs) (second number). Shadow shows SEMs. Dashed rectangle indicates stimulus window. Scale bars: 10 seconds (horizontal) and 0.5 normalized dF/F (vertical). Data from the same larva shown in a. d Mean intensity projection maps of ipsilateral(Ipsi)-contralateral(Contra) input selectivity of sensory-encoding ROIs. e Brainwide Ipsi-Contra input selectivity distributions of individual ROIs. f Regional means of Ipsi-Contra input selectivity. g Mean intensity projection maps of FIs. h Brainwide FIs distributions of individual ROIs. i Regional means of FIs. d–i Data are pooled across larvae (n = 4). The number of ROIs in d and e is 2301, and that in g and h is 1232. e, f, h, i The colors are coded accordingly to the color scale bars in d and g, respectively. e, h Horizontal lines: medians, 75 and 25 percentiles. Shadows of the violin plots scale according to the probability density function. f, i Each small dot representing one larva's value. Large dots, upper and lower limits of lines: medians, 75 and 25 percentiles, respectively. Scale bars in a, b, d, g 50 μm in Z-Brain atlas space. Source data are provided as a Source Data file. Credit: *Nature Communications* (2023). DOI: 10.1038/s41467-023-35836-2

Outlook

In this way, Samuel Sy and colleagues built on existing experimental advances established across the past decade within circuit neuroscience. They credit their research advances in part to newer methods that permit comprehensive behavioral monitoring and large-scale cellular-resolution of neuronal activities in diverse regions of the brain. The team developed an optofluidic method to assess chemosensory-mediated actions and brain-wide neural representations in larval zebrafish integrated with light-sheet fluorescence microscopy for whole brain imaging.

The microfluidics-based behavioral, chemical delivery and imaging principles demonstrated with Fish-on-Chips can be readily adapted to study chemosensory behaviors in several other organisms of similar size

or smaller length scales such as bacterial and larvae of drosophila as well. While wild animals in the scale of interest can navigate more complex odor landscapes, the Fish-on-Chips navigation platform offers a precisely regulated optofluidic setup to comparatively assess the neural representation of individual odors and detect the ensuing behavior of organisms. This experimental device will allow the team to gain deeper insights into the principles of sensory information processing.

More information: Sy et al, An optofluidic platform for interrogating chemosensory behavior and brainwide neural representation in larval zebrafish, *Nature Communications* (2023). DOI: 10.1038/s41467-023-35836-2

Fan Yang et al, Fish-on-a-chip: microfluidics for zebrafish research, *Lab on a Chip* (2016). DOI: 10.1039/C6LC00044D

© 2023 Science X Network

Citation: Fish-on-Chips: An optofluidic platform to investigate the neural and chemosensory axes of zebrafish (2023, January 27) retrieved 13 March 2024 from https://phys.org/news/2023-01-fish-on-chips-optofluidic-platform-neural-chemosensory.html

This document is subject to copyright. Apart from any fair dealing for the purpose of private study or research, no part may be reproduced without the written permission. The content is provided for information purposes only.